CHALMERS
UNIVERSITY OF TECHNOLOGY

Transient tire slip losses using the brush theory

Transient tyre slip losses using the brush theory

Luigi Romano*[a], Francesco Timpone[b], Fredrik Bruzelius[a,c], and Bengt Jacobson[a]

[a]Department of Mechanics and Maritime Sciences, Chalmers University of Technology, Hörsalsvägen 7A, 412 96 Gothenburg, Sweden
[b]Department of Industrial Engineering, University of Naples Federico II, Naples, Italy
[c]Driver and Vehicle, VTI Swedish National Road and Transport Research Institute, Box 8072, 402 78 Gothenburg, Sweden

Abstract

Tyre slip losses have been shown to have a significant impact on vehicles' performance in terms of energy efficiency, thus requiring accurate studies. In this paper, the transient dissipation mechanisms connected to the presence of micro-sliding phenomena occurring at the tyre-road interface are investigated analytically. The influence of a two-dimensional velocity field inside the contact patch is also considered resorting to the new brush theory recently developed by the authors. Theoretical results align with findings already known from literature, but suggest that the camber and turn spins contribute differently to the slip losses, and should be regarded as separate entities when the camber angle is sufficiently large. It also emerges from the present work that an additional amount of power which relates to the initial sliding conditions is generated or lost during the unsteady-state manoeuvres. A simple example is presented to illustrate the discrepancy between the microscopic and macroscopic approaches during a transient manoeuvre.

Keywords

Brush model, tyre models, transient tyre dynamics, energy losses, slip losses

1 Introduction

In recent years, the increasing commitment to more energy-efficient solutions aroused within both the industrial and academic vehicle dynamics communities a great interest in electric vehicles (EVs). These largely outperform conventional ones in terms of energy consumption, but at the same time have to face several issues connected to the well-known range-anxiety problem. In this context, it becomes even more crucial to minimise power losses in any form. In particular, in the generation process of traction and braking forces, pneumatic tyres dissipate power according to two different, fundamental mechanisms. The first kind of energy loss takes place mainly inside the rubber compound and connects directly to the viscoelastic nature of the material of which tyres are made. It is traditionally referred to as *rolling resistance*, and includes the contributions from both hysteresis and permanent plastic deformations which are not totally recovered during the rolling of the tyre. On the other hand, losses of the second type are caused by the existence of local sliding between the tread elements and the road, and are commonly referred to as *slip losses*. Opposed to the concept of rolling resistance, these may be interpreted as an interfacial, frictional dissipation. It has been shown that slip tyre losses may affect energy performance significantly [1, 2], thus deserving to be properly taken into account.

Some efforts have been thus directed to incorporate such losses when dealing with mathematical problems of energy efficiency optimisation. For example, Abe [3] focussed on tyre slip losses occurring in the sliding zone of the contact patch. In his analysis, he made use of the classic brush theory [4–7]. Conversely, Gruber [8] preferred an experimental approach and combined slip and powertrain dissipation. An analytical formulation of the driving resistance generated while cornering was proposed by Kobayashi et al [9, 10] and validated experimentally using a real vehicle equipped with four in-wheel motors. In [11], Torinsson solved analytically and numerical an optimisation problem in which the slip losses were modelled by using linear tyre forces.

*Corresponding author. Email: luigi.romano@chalmers.se.

From a purely theoretical perspective, slip losses have been investigated analytically within the context of both ground and railway vehicle dynamics. In particular, the computation of power dissipation due to finite sliding during the rolling contact can be performed following two different approaches. The first one, the so-called *macro approach*, is based on global equilibrium considerations. Accordingly, the power losses are calculated by considering the negative work done by the total generalised forces exerted at the tyre-road interface (longitudinal, lateral and self-aligning moment) for their dual entities (longitudinal, lateral and spin slip, respectively) [12, 13]. This approach has the advantage of being low-computationally costly, and therefore is often preferred when it comes to vehicle-dynamics simulations [14].

The second method is referred to as *micro approach*: the overall dissipation results from direct integration of the power density loss over the contact patch. The power losses at the microscopic level are due to the fact that the material points inflowing into the contact patch may have a relative local velocity with respect to the road (or the rail). The two approaches are often claimed to be consistent with each other, but systematic proof has been rarely attempted in the literature. In this sense, a recent result has been presented in [15], where the equivalence of the two methods has been shown by using classic brush models. The effect of the spin variable, however, has been disregarded in [15].

In this paper, the authors investigate the more general scenario of finite sliding by also considering the presence of large camber angles and turning speed. The present analysis is based on the novel transient brush theory developed by the authors in [16–18]. It is demonstrated that the micro and macro approaches are almost equivalent in the steady-state case, owing to very mild mathematical assumptions. A perfect agreement between the two formulations is found when the camber angle is sufficiently small to approximate the velocity field inside the contact patch with the tyre rolling speed.

The rest of this paper is organised as follows: in Sect. 2, the tyre-road contact mechanics equations are introduced and discussed in detail. The main assumptions in terms of boundary (BCs) and initial conditions (ICs) are stated formally. In Sect. 3, the analytical derivation for complete expression of the slip losses is carried out for the transient case, whereas Sect. 4 exemplifies the theory established in the paper and discusses the most relevant aspects connected to the transient effects. Finally, Sect. 5 summarises the main findings of the analysis and proposes some directions for further research.

2 Tyre-road contact mechanics equations

A reference frame $(O; x, y, z)$ with unit vectors $(\hat{\boldsymbol{e}}_x, \hat{\boldsymbol{e}}_y, \hat{\boldsymbol{e}}_z)$ is considered whose origin O coincides with the *contact point*[1]; the axes are oriented according to the SAE system: the x axis is directed towards the longitudinal direction of motion, the z axis points downward and the y axis lies in the road surface and is oriented so that the coordinate system is right-handed (Fig. 1).

The contact patch is defined mathematically as a closed set $\mathscr{P}$, whose interior and boundary are denoted with $\mathring{\mathscr{P}}$ and $\partial\mathscr{P}$, respectively. The contact patch collects all the points $\boldsymbol{x} \in \Pi$ of the tyre which make contact with the road, where $\Pi = \{x \in \mathbb{R}^3 \mid z = 0\}$ is the road plane. Both the tyre and the road are considered rigid once the normal contact has occurred. In particular, the road is modelled as a perfectly homogeneous, isotropic flat surface, without any irregularity; the tyre is also regarded as a rigid body, but anisotropy is allowed.

During the rolling of the tyre, a quantity evolves over the travelled distance $s = \int_0^t V_\mathrm{r}(t')\,\mathrm{d}t'$. Here, $V_\mathrm{r}(t) = \Omega(t)R_\mathrm{r}$ is the so-called *rolling speed*, and R_r denotes the *rolling radius* (usually greater than the tyre deformed radius). In particular, at each point $\boldsymbol{x} \in \mathscr{P}$ a nondimensional planar vector field $\mathrm{d}\boldsymbol{x}/\,\mathrm{d}s = \bar{\boldsymbol{v}}_{\boldsymbol{t}}(\boldsymbol{x}, s) = \bar{v}_x(\boldsymbol{x}, s)\hat{\boldsymbol{e}}_x + \bar{v}_y(\boldsymbol{x}, t)\hat{\boldsymbol{e}}_y$ and a finite vector displacement $\boldsymbol{u}_{\boldsymbol{t}}(\boldsymbol{x}, s) = u_x(\boldsymbol{x}, s)\hat{\boldsymbol{e}}_x + u_y(\boldsymbol{x}, s)\hat{\boldsymbol{e}}_y$ are associated, the latter representing the relative deformation of the material point located at the coordinate $\boldsymbol{x}$ with respect to its initial configuration. In the brush model, the deformation of a material point is also interpreted as the deformation of a *bristle* attached to the wheel rim; hence, the vector $\boldsymbol{u}_{\boldsymbol{t}}(\boldsymbol{x}, s)$ is equivalently referred to as the tangential deformation, deflection or displacement of a bristle. Each bristle may be also subjected to a planar force per unit of area $\boldsymbol{q}_{\boldsymbol{t}}(\boldsymbol{x}, s) = q_x(\boldsymbol{x}, s)\hat{\boldsymbol{e}}_x + q_y(\boldsymbol{x}, s)\hat{\boldsymbol{e}}_y$, called tangential shear stress.

The relative speed between a bristle inside the contact patch and the road in the plane is called *micro-sliding velocity* and indicated with $\boldsymbol{v}_\mathrm{s}(\boldsymbol{x}, s) = v_{\mathrm{s}x}\hat{\boldsymbol{e}}_x + v_{\mathrm{s}y}\hat{\boldsymbol{e}}_y$. Adopting the simplest Coulomb friction model, the fundamental equations governing the tyre-road contact mechanics may be formulated

[1] This point lies in the vertical plane that contains the wheel centre and the point of intersection between the wheel rotational axis and the road. Usually, it is also chosen so that it separates the section of the contact patch into two equal semi-widths (see [4] for further clarifications).

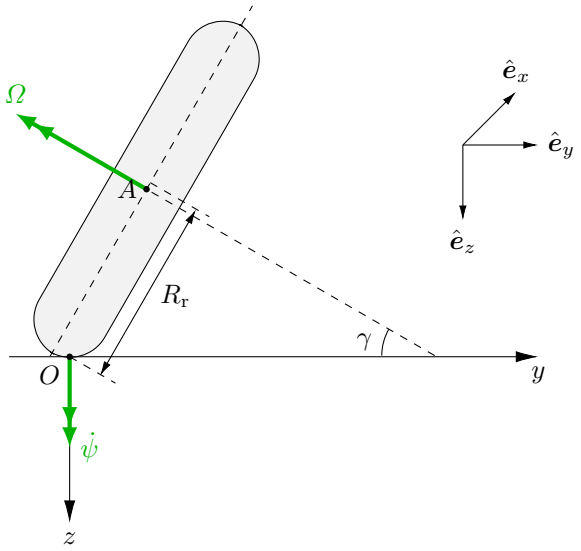

Figure 1: Tyre reference frame with angular velocities.

as

$$\bar{\boldsymbol{v}}_\mathrm{s}(\boldsymbol{x},s)=\boldsymbol{0} \implies q_{\boldsymbol{t}}(\boldsymbol{x},s)\leq\mu q_z(\boldsymbol{x}), \tag{1a}$$

$$\boldsymbol{q}_{\boldsymbol{t}}(\boldsymbol{x},s)=-\mu q_z(\boldsymbol{x})\frac{\bar{\boldsymbol{v}}_\mathrm{s}(\boldsymbol{x},s)}{\bar{v}_\mathrm{s}(\boldsymbol{x},s)} \iff \bar{\boldsymbol{v}}_\mathrm{s}(\boldsymbol{x},s)\neq\boldsymbol{0}, \tag{1b}$$

where[2] $q_{\boldsymbol{t}}(\boldsymbol{x},t)=\big\|\boldsymbol{q}_{\boldsymbol{t}}(\boldsymbol{x},t)\big\|$, $\bar{v}_\mathrm{s}(\boldsymbol{x},t)=\big\|\bar{\boldsymbol{v}}_\mathrm{s}(\boldsymbol{x},t)\big\|$ and $\bar{\boldsymbol{v}}_\mathrm{s}(\boldsymbol{x},s)=\boldsymbol{v}_\mathrm{s}(\boldsymbol{x},s)/V_\mathrm{r}(s)$. Finally, $q_z(\boldsymbol{x})$ is the vertical pressure acting at the coordinate $\boldsymbol{x}$. To solve the above Eqs. (1), two other sets of relationships are needed: the *tyre-road kinematic equations* and the *constitutive relations*. The first set prescribes a relation between the sliding speed and the deformation of the tyre inside the contact patch; the latter the relation between the aforementioned deformation and the tangential stress acting on each material point.

2.1 Tyre-road kinematic equations

The tyre-road kinematic equations in their complete form may be found in many reference textbooks, for example [4, 6, 7]. The notation used in this paper follows that of Romano et al. [17–19]. In particular, expressing each variable as a function of the travelled distance s, the following system of PDEs is obtained:

$$\bar{\boldsymbol{v}}_\mathrm{s}(\boldsymbol{x},t)=-\boldsymbol{\sigma}(s)-\mathbf{A}_\varphi(s)\big(\boldsymbol{x}+\chi_\psi(s)\boldsymbol{u}_{\boldsymbol{t}}(\boldsymbol{x},s)\big)+\frac{\partial\boldsymbol{u}_{\boldsymbol{t}}(\boldsymbol{x},s)}{\partial s}+\big(\bar{\boldsymbol{v}}_{\boldsymbol{t}}(\boldsymbol{x},s)\cdot\nabla_{\boldsymbol{t}}\big)\boldsymbol{u}_{\boldsymbol{t}}(\boldsymbol{x},s),\quad(\boldsymbol{x},s)\in\mathring{\mathscr{P}}\times\mathbb{R}_{>0}, \tag{2}$$

where the nondimensional tangential velocity field $\bar{\boldsymbol{v}}_{\boldsymbol{t}}(\boldsymbol{x},s)=\bar{v}_x(y,s)\hat{\boldsymbol{e}}_x+\bar{v}_y(x,s)\hat{\boldsymbol{e}}_y$ reads in components

$$\bar{v}_x(y,s)=-1+\varphi_\gamma(s)y, \tag{3a}$$

$$\bar{v}_y(x,s)=-\varphi_\gamma(s)x, \tag{3b}$$

and the tangential gradient $\nabla_{\boldsymbol{t}}$ collects the tangential partial derivatives, that is $\nabla_{\boldsymbol{t}}\triangleq\begin{bmatrix}\partial/\partial x & \partial/\partial y\end{bmatrix}^\mathrm{T}$. It should be noticed that, for sake of simplicity, the (small) contribution of $\dot{\gamma}(s)$ on the derivative $\mathrm{d}y/\,\mathrm{d}s$ in Eqs. (3)[3] has been neglected. This is justifiable and connected with the small instantaneous or so-called non-lagging response to camber changes. Further details about this phenomenon are given in [4].

The translational slip $\boldsymbol{\sigma}(s)$ and the *spin tensor* $\mathbf{A}_\varphi(s)$ in Eq. (2) read

$$\boldsymbol{\sigma}(s)=\sigma_x(s)\hat{\boldsymbol{e}}_x+\sigma_y(s)\hat{\boldsymbol{e}}_y, \tag{4a}$$

[2] In this paper, with some abuse of notation, $\|\cdot\|$ is used in place $\|\cdot\|_2$.
[3] Note that this does not affect the results in Sect. 3.

$$\mathbf{A}_{\varphi}(s) \triangleq \begin{bmatrix} 0 & -\varphi(s) \\ \varphi(s) & 0 \end{bmatrix}, \tag{4b}$$

where $\sigma_x(s)$ and $\sigma_y(s)$ are the *theoretical longitudinal* and *lateral slip*, whilst $\varphi(s)$ is addressed to both as *rotational slip* or *spin*. In turn, the spin parameter φ may be decomposed in its two contribution by defining

$$\varphi_\gamma(s) = \chi_\gamma(s)\varphi(s) = \frac{1}{R_\mathrm{r}}\big(1-\varepsilon_\gamma\big)\sin\gamma(s), \qquad \varphi_\psi(s) = \chi_\psi(s)\varphi(s) = -\frac{\dot{\psi}(s)}{V_\mathrm{r}(s)}, \tag{5a}$$

which are called *camber* and *turn spin*, respectively. These two parameters may be interpreted as two different signed curvatures to which the tyre path is subjected. The ratios $\chi_\gamma(s)$ and $\chi_\psi(s)$ have been introduced in Romano et al. [17] and are simply called *camber* and *turn ratio*; they are chosen such that $\chi_\gamma(s)+\chi_\psi(s)=1$ and thus also $\varphi_\gamma(s)+\varphi_\psi(s)=\varphi(s)$. The quantities $\gamma(s)$ and $\dot{\psi}(s)$ showing in (5) are the camber angle and the turning speed. Finally, the parameter ε_γ is known in the literature as *camber reduction factor* and it may be assumed to be almost constant for a tyre [4, 6, 20].

2.2 Constitutive relationships

These equations establish the relationships between the local shear stress $\boldsymbol{q_t}(\boldsymbol{x},s)$ acting in the contact patch and the bristle deflection $\boldsymbol{u_t}(\boldsymbol{x},s)$. In spite of the viscoelastic nature of the tyre, for sake of simplicity it has been commonly established in the literature to assume linear elasticity [5], i.e. a constitutive relation of the type

$$\boldsymbol{q_t}(\boldsymbol{x},s) = \mathbf{K_t}\boldsymbol{u_t}(\boldsymbol{x},s), \tag{6}$$

where the tangential stiffness matrix $\mathbf{K_t}$ is often assumed to be diagonal. In this paper, $\mathbf{K_t}$ is only required to be a self-adjoint operator. This property is implied by the following Assumption 2.1.

Assumption 2.1. *The tangential stiffness matrix $\mathbf{K_t}$ is real and symmetric.*

2.3 Equilibrium relationships

The following equations establish the relationships between the local shear stresses arising inside the contact patch and the forces and moment acting on the tyre. By integration[4]:

$$\boldsymbol{F_t}\big(\boldsymbol{\sigma},\varphi_\gamma,\varphi_\psi,s\big) = \iint_{\mathscr{P}} \boldsymbol{q_t}\big(\boldsymbol{x},s;\boldsymbol{\sigma},\varphi_\gamma,\varphi_\psi\big)\,\mathrm{d}\boldsymbol{x}, \tag{7a}$$

$$\begin{aligned} M_z\big(\boldsymbol{\sigma},\varphi_\gamma,\varphi_\psi,s\big) = &\iint_{\mathscr{P}} \big(x+u_x(\boldsymbol{x},s)\big) q_y\big(\boldsymbol{x},s;\boldsymbol{\sigma},\varphi_\gamma,\varphi_\psi\big)\,\mathrm{d}\boldsymbol{x} \\ &- \iint_{\mathscr{P}} \big(y+u_y(\boldsymbol{x},s)\big) q_x\big(\boldsymbol{x},s;\boldsymbol{\sigma},\varphi_\gamma,\varphi_\psi\big)\,\mathrm{d}\boldsymbol{x}. \end{aligned} \tag{7b}$$

2.4 Boundary and initial conditions

In formulating the boundary and initial conditions to the problem, a constant shape for the contact patch $\mathscr{P}$ is assumed. In particular, Eqs. (2) are two coupled PDEs – more specifically, *linear transport equations* – defined on a bounded open domain $\mathring{\mathscr{P}}$. Thus, to guarantee the uniqueness of the solution, a proper BC and an initial condition (IC) need to be prescribed. Before stating the BC, the notions of *leading edge* $\mathscr{L}$, *neutral edge* $\mathscr{N}$ and *trailing edge* $\mathscr{T}$ [17, 18] may be introduced as follows:

$$\mathscr{L} \triangleq \Big\{ \boldsymbol{x} \in \partial\mathscr{P} \;\Big|\; \bar{\boldsymbol{v}}_{\boldsymbol{t}}(\boldsymbol{x},s)\cdot\hat{\boldsymbol{\nu}}_{\partial\mathscr{P}}(\boldsymbol{x}) < 0 \Big\}, \tag{8a}$$

$$\mathscr{N} \triangleq \Big\{ \boldsymbol{x} \in \partial\mathscr{P} \;\Big|\; \bar{\boldsymbol{v}}_{\boldsymbol{t}}(\boldsymbol{x},s)\cdot\hat{\boldsymbol{\nu}}_{\partial\mathscr{P}}(\boldsymbol{x}) = 0 \Big\}, \tag{8b}$$

$$\mathscr{T} \triangleq \Big\{ \boldsymbol{x} \in \partial\mathscr{P} \;\Big|\; \bar{\boldsymbol{v}}_{\boldsymbol{t}}(\boldsymbol{x},s)\cdot\hat{\boldsymbol{\nu}}_{\partial\mathscr{P}}(\boldsymbol{x}) > 0 \Big\}, \tag{8c}$$

where the unit vector $\hat{\boldsymbol{\nu}}_{\partial\mathscr{P}}(\boldsymbol{x})$ represents the outer-pointing unit normal which lies in the plane $z=0$. It should be noticed that the scalar product $\bar{\boldsymbol{v}}_{\boldsymbol{t}}(\boldsymbol{x},s)\cdot\hat{\boldsymbol{\nu}}_{\partial\mathscr{P}}(\boldsymbol{x})$ represents the elementary flow of the bristles through the boundary $\partial\mathscr{P}$ of the contact patch.

[4] When integrating over $\mathscr{P}$, it is written, with some abuse of notation, $\mathrm{d}\boldsymbol{x} = \mathrm{d}x\,\mathrm{d}y$, since z is fixed.

Indeed, the classic brush theory, assuming uncoupled bristles, prescribes the continuity of the shear stress at the interface between the traction-free portion of the road, that is the part which is not making contact with the tyre, and the interior of contact area. If a pure elastic constitutive relation is assumed, the direct consequence is that the bristles inflowing into the contact patch must enter undeformed. This can be stated in mathematical terms as

$$\text{BC:} \qquad \boldsymbol{q_t}(\boldsymbol{x},s) = \mathbf{K_t}\boldsymbol{u_t}(\boldsymbol{x},s) = \mathbf{0} \iff \boldsymbol{u_t}(\boldsymbol{x},s) = \mathbf{0}, \qquad (\boldsymbol{x},s) \in \mathscr{L} \times \mathbb{R}_{>0}. \tag{9}$$

Basically, the previous relation imposes that the bristles must enter the contact patch undeformed, since the points $\boldsymbol{x} \in \mathscr{L}$ are the points inflowing into the contact patch $\mathscr{P}$. The above BCs (8a) ensure the well-posedness of the *free* problem under *vanishing sliding* assumptions (that is full adhesion over the contact patch) and constant contact shape, and therefore it is often argued that inflow boundaries are, to some extent, the natural boundaries for transport equations [21, 22]. The additional Assumption 2.2 is introduced.

Assumption 2.2. *For every $\boldsymbol{x} \in \partial\mathscr{P}$, we assume that at least one of the the two following conditions is fulfilled for every $s \in \mathbb{R}_{\geq 0}$:*

$$\bar{\boldsymbol{v}}_{\boldsymbol{t}}(\boldsymbol{x},s) \cdot \hat{\boldsymbol{\nu}}_{\partial\mathscr{P}}(\boldsymbol{x}) = 0, \tag{10a}$$

$$q_z(\boldsymbol{x},s) = 0. \tag{10b}$$

The requirement above is needed to ensure that $q_{\boldsymbol{t}}(\boldsymbol{x},s) = 0$ for all $\boldsymbol{x} \in \partial\mathscr{P}$ where the product $\bar{\boldsymbol{v}}_{\boldsymbol{t}}(\boldsymbol{x},s) \cdot \hat{\boldsymbol{\nu}}_{\partial\mathscr{P}}(\boldsymbol{x})$ does not vanish. In particular, Assumption 2.2 ensures that $\boldsymbol{u_t}(\boldsymbol{x},s) = \mathbf{0}$ on $\mathscr{T}$ (it should be observed that the BC (9) already prescribes $\boldsymbol{u_t}(\boldsymbol{x},s) = \mathbf{0}$ on $\mathscr{L}$.).

From a physical perspective, this is legitimated by the fact that the vertical pressure must be zero on the boundary of $\mathscr{P}$, i.e. $q_z(\boldsymbol{x},s) = 0$ on $\partial\mathscr{P}$, thus separating two regions of the tyre which are not in contact with the road. However, more practical aspects should be addressed when dealing with the simplified brush theory. For car and truck tyres, in fact, the contact patch is almost exclusively assumed to be rectangular in shape, with a vertical pressure distribution satisfying Assumption 2.2 only at the leading and trailing edges.

Two classic examples of contact geometries and pressure distributions satisfying Assumption 2.2 are given below.

Example 2.3 (Rectangular contact patch)**.** For a rectangular contact patch given by

$$\mathscr{P} \triangleq \big\{\boldsymbol{x} \in \Pi \;\big|\; -a \leq x \leq a,\, -b \leq y \leq b\big\}, \tag{11}$$

the simplest pressure distribution may be assumed of the type

$$q_z(x) = q_z^*\left[1 - \left(\frac{x}{a}\right)^2\right], \tag{12}$$

with $q_z^* \triangleq 3F_z/(8ab)$, where F_z is the total vertical load acting on the tyre. Clearly, a pressure distribution as in Eq. (12) is strictly concave and attains zero values at $x = x_{\mathscr{L}} = a$ and $x = x_{\mathscr{T}} = -a$, which correspond to the leading and trailing edges, respectively. It should be observed that the contact shape (11) together with the pressure distribution (12) only satisfies Assumption 2.2 with the approximated nondimensional velocity field $\bar{\boldsymbol{v}}_{\boldsymbol{t}}(\boldsymbol{x},s) = -V_{\mathrm{r}}(s)\hat{\boldsymbol{e}}_x$, as in the classic brush theory. The limitation of such geometry are discussed in [17, 18].

Example 2.4 (Elliptical contact patch)**.** An elliptical contact patch may be described mathematically as

$$\mathscr{P} \triangleq \left\{\boldsymbol{x} \in \Pi \;\middle|\; \frac{x^2}{a^2} + \frac{y^2}{b^2} \leq 1\right\}, \tag{13}$$

with the leading and trailing edges reading respectively[5] $x = x_{\mathscr{L}}(y) = a\sqrt{1 - \dfrac{y^2}{b^2}}$ and $x = x_{\mathscr{T}}(y) = -a\sqrt{1 - \dfrac{y^2}{b^2}}$. A parabolic pressure distribution may be hence assumed of the type

$$q_z(\boldsymbol{x}) = q_z^*\left(1 - \frac{x^2}{a^2} - \frac{y^2}{b^2}\right), \tag{14}$$

[5]It is possible to show that the leading and trailing edges admit this representation if $\dfrac{a^2}{b} - b \leq \dfrac{1}{|\varphi_\gamma|}$.

where $q_z^* \triangleq 2F_z/(\pi ab)$. An elliptical contact patch with vertical pressure given by (14) satisfies Assumption 2.2 on the whole boundary $\partial\mathscr{P}$.

As far as the IC is concerned, it is convenient in first approximation to pretend that the initial distribution is known on the whole contact patch under *vanishing sliding* conditions. In this case, the IC may be formulated on the whole interior $\mathring{\mathscr{P}}$ of the domain $\mathscr{P}$:

$$\text{IC:} \qquad \boldsymbol{u_t}(\boldsymbol{x},0) = \boldsymbol{u_{t0}}(\boldsymbol{x}), \qquad \boldsymbol{x} \in \mathring{\mathscr{P}}, \tag{15}$$

for any $\boldsymbol{u_{t0}}(\boldsymbol{x}) \in C^1(\mathring{\mathscr{P}})$, even though initial distributions which are only $C^0(\mathring{\mathscr{P}})$ should be allowed[6]. Clearly, it must be $\boldsymbol{u_{t0}}(\boldsymbol{x})\big|_{\mathscr{L}} = \boldsymbol{0}$ following from frictional considerations.

The notions of *sliding* and *adhesion edge* $\mathscr{S}$ and $\mathscr{A}$ need also to be introduced. In transient conditions, they may be both dependent on the travelled distance s (see Appendix A). More specifically, the former represents the transition curve which separates the adhesion solution from the sliding one in presence of limited friction, and may be described mathematically as the implicit curve for which the condition $\left\|\mathbf{K_t}\boldsymbol{u_t}^{(\mathrm{a})}(\boldsymbol{x},s)\right\| - \mu q_z(\boldsymbol{x},s) = 0$ is fulfilled. The adhesion edge, instead, collects the points for which the sliding speed tends again to zero and adhesion is restored starting from a previous sliding solution. A more detailed discussion is outlined in [18]. This paper restricts itself to state the corresponding BCs from adhesion to sliding:

$$\text{BC:} \qquad \boldsymbol{u_t}^{(\mathrm{s})}(\boldsymbol{x},s)\Big|_{\mathscr{S}(s)} = \mathbf{K_t}^{-1}\mu q_z(\boldsymbol{x},s)\hat{\boldsymbol{s}}_{\boldsymbol{t}}(\boldsymbol{x},s)\Big|_{\mathscr{S}(s)} = \boldsymbol{u_t}^{(\mathrm{a})}(\boldsymbol{x},s)\Big|_{\mathscr{S}(s)}, \qquad s \in \mathbb{R}_{>0}, \tag{16}$$

and from sliding to adhesion:

$$\text{BC:} \qquad \boldsymbol{u_t}^{(\mathrm{a})}(\boldsymbol{x},s)\Big|_{\mathscr{A}(s)} = \boldsymbol{u_t}^{(\mathrm{s})}(\boldsymbol{x},s)\Big|_{\mathscr{A}(s)}, \qquad s \in \mathbb{R}_{>0}. \tag{17}$$

Both (16) and (17) ensure the continuity of the displacements.

3 Theoretical analysis of tyre slip losses

The authors of this paper move now to derive an analytical expression for the slip losses $P_{\mathrm{s}}(s)$ due to the existence of micro-sliding phenomena inside the contact patch. The computation is carried out by integration over $\mathscr{P}$. To this extent, the contact patch, assumed constant in shape, is partitioned into different subdomains, where different solutions apply depending on the geometry of the boundary $\partial\mathscr{P}$. This is assumed to be sufficiently regular to allow for solutions which are uniquely defined. It should be noticed that the form of the boundaries separating these domains are, at least in theory, known *a priori*[7] as integral solutions of $\mathrm{d}\boldsymbol{x}(s)/\,\mathrm{d}s = \bar{\boldsymbol{v}}_{\boldsymbol{t}}(\boldsymbol{x},s)$. Furthermore, it follows from the well-posedness of the problem at hand that trajectories $\boldsymbol{x}(s)$ originating from different initial conditions $\boldsymbol{x}_0$ never cross each other, and thus these domains may always be determined uniquely[8]. Subpartition of these, denoted with $\mathscr{P}_i$ ($i \in \mathcal{I}$), should be chosen such that, in turn, every $\mathscr{P}_i$ ($i \in \mathcal{I}$) may be divided into adhesion and sliding zones which may be numbered consecutively. Since, in the case of limited friction, for each sliding zone a previous adhesion zone must exist, it is possible to resort to some index $j \in \mathcal{J}_i$, with $\mathcal{J}_i$ dependent on the index i, and denote by $\mathscr{P}_{ij}$ the generic subdomain of the contact patch and by $\mathscr{P}_{ij}^{(\mathrm{a})}$ and $\mathscr{P}_{ij}^{(\mathrm{s})}$ its adhesion and sliding areas, respectively.

Of course, it holds that $\mathscr{P} = \bigcup_{i\in\mathcal{I}}\bigcup_{j\in\mathcal{J}_i}\left(\mathscr{P}_{ij}^{(\mathrm{a})} \cup \mathscr{P}_{ij}^{(\mathrm{s})}\right)$. In each subdomain, the displacements $\boldsymbol{u_t}(\boldsymbol{x},s)$, the vertical pressure distribution $q_z(\boldsymbol{x},s)$ and the edges $\mathscr{S}_{ij}(s)$ and $\mathscr{A}_{ij}(s)$ may be assumed sufficiently smooth for what follows in the derivation of the result. It is worth noticing that the edges $\mathscr{S}_{ij}(s)$ and $\mathscr{A}_{ij}(s)$ are allowed to travel inside the contact patch with unknown nondimensional velocity, which must

[6] In this case, we refer to *weak* solutions over the whole contact patch.

[7] Provided that the camber spin $\varphi_\gamma(s)$ and the camber itself are independent of the bristle displacement.

[8] When restricting the attention to the solution of the system $\mathrm{d}\boldsymbol{x}(s)/\,\mathrm{d}s = \bar{\boldsymbol{v}}_{\boldsymbol{t}}(\boldsymbol{x},s)$, the well-posedness of the problem generally stems from consideration about the regularity of the right-hand sides of Eqs. (3), which in the present case are clearly globally Lipschitz-continuous in the independent variable, with Lipschitz constant $L = \varphi_\gamma^{\max}$. Indeed, it is $\left\|\bar{\boldsymbol{v}}_{\boldsymbol{t}}(\boldsymbol{x}_1,s) - \bar{\boldsymbol{v}}_{\boldsymbol{t}}(\boldsymbol{x}_1,s)\right\| = \left|\varphi_\gamma(s)\right|\|\boldsymbol{x}_1 - \boldsymbol{x}_2\| \le \varphi_\gamma^{\max}\|\boldsymbol{x}_1 - \boldsymbol{x}_2\|$, where $\varphi_\gamma^{\max} \triangleq (1-\varepsilon_\gamma)/R_{\mathrm{r}}$ is the limit value for the camber spin and is given by physical considerations.

be deduced formally from the displacements $\boldsymbol{u_t}(\boldsymbol{x}, s)$. For a detailed discussion, the reader is referred to Appendix A[9].

The total power losses may now be computed by integration over $\mathscr{P}$ of the power loss density $p_{\mathrm{s}}(\boldsymbol{x}, s)$, given by the product between the tangential stress and the micro-sliding velocity $\boldsymbol{q_t}(\boldsymbol{x}, s) \cdot \boldsymbol{v}_{\mathrm{s}}(\boldsymbol{x}, s)$. This yields

$$\begin{aligned} P_{\mathrm{s}}(s) = \iint_{\mathscr{P}} p_{\mathrm{s}}(\boldsymbol{x}, s)\,\mathrm{d}\boldsymbol{x} &= \iint_{\mathscr{P}} \boldsymbol{q_t}(\boldsymbol{x}, s) \cdot \boldsymbol{v}_{\mathrm{s}}(\boldsymbol{x}, s)\,\mathrm{d}\boldsymbol{x} = V_{\mathrm{r}}(s) \iint_{\mathscr{P}(s)} \boldsymbol{q_t}(\boldsymbol{x}, s) \cdot \bar{\boldsymbol{v}}_{\mathrm{s}}(\boldsymbol{x}, s)\,\mathrm{d}\boldsymbol{x} \\ &= V_{\mathrm{r}}(s) \iint_{\mathscr{P}} \boldsymbol{q_t}(\boldsymbol{x}, s) \cdot \left[\frac{\partial \boldsymbol{u_t}(\boldsymbol{x}, s)}{\partial s} + \big(\bar{\boldsymbol{v}}_{\boldsymbol{t}}(\boldsymbol{x}, s) \cdot \nabla_{\boldsymbol{t}}\big) \boldsymbol{u_t}(\boldsymbol{x}, s) \right] \mathrm{d}\boldsymbol{x} \\ &\quad - V_{\mathrm{r}}(s) \iint_{\mathscr{P}} \boldsymbol{q_t}(\boldsymbol{x}, s) \cdot \Big[\boldsymbol{\sigma}(s) + \mathbf{A}_{\varphi}\big(\boldsymbol{x} + \chi_{\psi} \boldsymbol{u_t}(\boldsymbol{x}, s)\big) \Big]\,\mathrm{d}\boldsymbol{x}. \end{aligned} \tag{18}$$

By virtue of (7), the above expression may be restated more compactly as

$$\begin{aligned} P_{\mathrm{s}}(s) = V_{\mathrm{r}}(s) \iint_{\mathscr{P}} \boldsymbol{q_t}(\boldsymbol{x}, s)\, \frac{\partial \boldsymbol{u_t}(\boldsymbol{x}, s)}{\partial s}\,\mathrm{d}\boldsymbol{x} + V_{\mathrm{r}}(s) \iint_{\mathscr{P}} \boldsymbol{q_t}(\boldsymbol{x}, s) \cdot \big(\bar{\boldsymbol{v}}_{\boldsymbol{t}}(\boldsymbol{x}, s) \cdot \nabla_{\boldsymbol{t}}\big) \boldsymbol{u_t}(\boldsymbol{x}, s)\,\mathrm{d}\boldsymbol{x} \\ - P_{\boldsymbol{\sigma}}(s) - P_{\varphi}(s) + P_{\gamma}^{(\epsilon)}(s), \end{aligned} \tag{19}$$

where the following quantities have been defined:

$$P_{\boldsymbol{\sigma}}(s) \triangleq V_{\mathrm{r}}(s) \boldsymbol{F_t}(s) \cdot \boldsymbol{\sigma}(s), \tag{20a}$$

$$P_{\varphi}(s) \triangleq V_{\mathrm{r}}(s) M_z(s) \varphi(s), \tag{20b}$$

$$P_{\gamma}^{(\epsilon)}(s) \triangleq \varphi_{\gamma}(s) V_{\mathrm{r}}(s) \iint_{\mathscr{P}(s)} q_y(\boldsymbol{x}, s) u_x(\boldsymbol{x}, s) - q_x(\boldsymbol{x}, s) u_y(\boldsymbol{x}, s)\,\mathrm{d}\boldsymbol{x}. \tag{20c}$$

To derive the final expression for the total slip losses, the two integrals on the right-hand side of (19) need to be restated into a more useful form. Starting from the first one, it follows from Assumption 2.1 that

$$V_{\mathrm{r}}(s) \iint_{\mathscr{P}} \boldsymbol{q_t}(\boldsymbol{x}, s) \cdot \frac{\partial \boldsymbol{u_t}(\boldsymbol{x}, s)}{\partial s}\,\mathrm{d}\boldsymbol{x} = \frac{1}{2} V_{\mathrm{r}}(s) \iint_{\mathscr{P}} \frac{\partial}{\partial s} \left[\boldsymbol{q_t}(\boldsymbol{x}, s) \cdot \boldsymbol{u_t}(\boldsymbol{x}, s) \right] \mathrm{d}\boldsymbol{x}. \tag{21}$$

A reverse application of Leibniz rule also yields

$$\begin{aligned} \iint_{\mathscr{P}} \frac{\partial}{\partial s} \left[\boldsymbol{q_t}(\boldsymbol{x}, s) \cdot \boldsymbol{u_t}(\boldsymbol{x}, s) \right] \mathrm{d}\boldsymbol{x} &= \frac{\mathrm{d}}{\mathrm{d}s} \iint_{\mathscr{P}} \boldsymbol{q_t}(\boldsymbol{x}, s) \cdot \boldsymbol{u_t}(\boldsymbol{x}, s)\,\mathrm{d}\boldsymbol{x} \\ &\quad - \sum_{i \in \mathcal{I}} \sum_{j \in \mathcal{J}_i} \oint_{\partial \mathscr{P}_{ij}^{(\mathrm{a})}(s)} \Big[\boldsymbol{q}_{ij\boldsymbol{t}}^{(\mathrm{a})}(\boldsymbol{x}, s) \cdot \boldsymbol{u}_{ij\boldsymbol{t}}^{(\mathrm{a})}(\boldsymbol{x}, s) \Big] \bar{\boldsymbol{v}}_{\partial \mathscr{P}_{ij}^{(\mathrm{a})}}(\boldsymbol{x}, s) \cdot \hat{\boldsymbol{\nu}}_{\partial \mathscr{P}_{ij}^{(\mathrm{a})}}(\boldsymbol{x}, s)\,\mathrm{d}L \\ &\quad - \sum_{i \in \mathcal{I}} \sum_{j \in \mathcal{J}_i} \oint_{\partial \mathscr{P}_{ij}^{(\mathrm{s})}(s)} \Big[\boldsymbol{q}_{ij\boldsymbol{t}}^{(\mathrm{s})}(\boldsymbol{x}, s) \cdot \boldsymbol{u}_{ij\boldsymbol{t}}^{(\mathrm{s})}(\boldsymbol{x}, s) \Big] \bar{\boldsymbol{v}}_{\partial \mathscr{P}_{ij}^{(\mathrm{s})}}(\boldsymbol{x}, s) \cdot \hat{\boldsymbol{\nu}}_{\partial \mathscr{P}_{ij}^{(\mathrm{s})}}(\boldsymbol{x}, s)\,\mathrm{d}L. \end{aligned} \tag{22}$$

To simplify the above Eq. (22), the contribution due to each term in the summations should be analysed separately. In fact, these represent the line integrals on the boundaries of each subdomain of $\mathscr{P}$. For any curve (or portion of curve) which belongs to $\partial\mathscr{P}$, it is either $\bar{\boldsymbol{v}}_{\partial\mathscr{P}}(\boldsymbol{x}) \cdot \hat{\boldsymbol{\nu}}_{\partial\mathscr{P}}(\boldsymbol{x}) = 0$ or $\boldsymbol{u_t}(\boldsymbol{x}, s) = \boldsymbol{0}$ by Assumption 2.2. Indeed, any $\boldsymbol{x}$ such that $\boldsymbol{u_t}(\boldsymbol{x}, s) \neq \boldsymbol{0}$ belongs to the neutral edge $\boldsymbol{x} \in \mathscr{N}$, and therefore the vector fields $\bar{\boldsymbol{v}}_{\boldsymbol{t}}(\boldsymbol{x}, s)$ and $\bar{\boldsymbol{v}}_{\partial \mathscr{P}_{ij}^{(\mathrm{s})}}(\boldsymbol{x}, s)$ need to be parallel, which implies $\bar{\boldsymbol{v}}_{\partial \mathscr{P}_{ij}^{(\mathrm{s})}}(\boldsymbol{x}, s) \cdot \hat{\boldsymbol{\nu}}_{\partial \mathscr{P}_{ij}^{(\mathrm{s})}}(\boldsymbol{x}, s) = 0$. The same happens for any curve which separates a domain $\mathscr{P}_{ij}$ from the adjacent domains $\mathscr{P}_{i+1j}$ or $\mathscr{P}_{i-1j}$ for which the displacement is discontinuous at the interface. Indeed, such boundaries are characteristics, and are given by the integral solutions to $\mathrm{d}\boldsymbol{x}(s)/\,\mathrm{d}s = \bar{\boldsymbol{v}}_{\boldsymbol{t}}(\boldsymbol{x}, s)$. Therefore, the normal at any point is always orthogonal to the nondimensional velocity field $\bar{\boldsymbol{v}}_{\boldsymbol{t}}(\boldsymbol{x}, s)$. With this reasoning, it is easy to show

[9] Another technical consideration is that, as it is defined, a sliding region $\mathscr{P}_{ij}^{(\mathrm{s})}$ must not be necessarily compact. For what follows, the *compact* version of such $\mathscr{P}_{ij}^{(\mathrm{s})}$ may be considered, and therefore also the extension of the corresponding sliding solution $\boldsymbol{u}_{ij\boldsymbol{t}}^{(\mathrm{s})}(\boldsymbol{x}, s)$. This is always possible, since the sliding solution $\boldsymbol{u}_{ij\boldsymbol{t}}^{(\mathrm{s})}(\boldsymbol{x}, s)$ is continuous by assumption on the adhesion and sliding edges.

that Eq. (22) turns into

$$\begin{aligned}\iint_{\mathscr{P}} \frac{\partial}{\partial s}\left[\boldsymbol{q_t}(\boldsymbol{x},s)\cdot\boldsymbol{u_t}(\boldsymbol{x},s)\right]\mathrm{d}\boldsymbol{x} &= \frac{\mathrm{d}}{\mathrm{d}s}\iint_{\mathscr{P}} \boldsymbol{q_t}(\boldsymbol{x},s)\cdot\boldsymbol{u_t}(\boldsymbol{x},s)\,\mathrm{d}\boldsymbol{x}\\ &-\sum_{i\in\mathcal{I}}\sum_{j\in\mathcal{J}_i}\int_{\mathscr{S}_{ij}(s)}\left[\!\left[\boldsymbol{q}_{ij\boldsymbol{t}}(\boldsymbol{x},s)\cdot\boldsymbol{u}_{ij\boldsymbol{t}}(\boldsymbol{x},s)\right]\!\right]_{\mathscr{S}_{ij}(s)}\bar{\boldsymbol{v}}_{\mathscr{S}_{ij}}(\boldsymbol{x},s)\cdot\hat{\boldsymbol{\nu}}_{\mathscr{S}_{ij}}(\boldsymbol{x},s)\,\mathrm{d}L\\ &-\sum_{i\in\mathcal{I}}\sum_{j\in\mathcal{J}_i|j>1}\int_{\mathscr{A}_{ij}(s)}\left[\!\left[\boldsymbol{q}_{ij\boldsymbol{t}}(\boldsymbol{x},s)\cdot\boldsymbol{u}_{ij\boldsymbol{t}}(\boldsymbol{x},s)\right]\!\right]_{\mathscr{A}_{ij}(t)}\bar{\boldsymbol{v}}_{\mathscr{A}_{ij}}(\boldsymbol{x},s)\cdot\hat{\boldsymbol{\nu}}_{\mathscr{A}_{ij}}(\boldsymbol{x},s)\,\mathrm{d}L,\end{aligned} \tag{23}$$

where in the brackets $[\![\cdot]\!]$ represent the sudden transition of the deflected bristle (i.e. the jump between the deflection of the bristle) from adhesion to sliding and *vice versa*. More specifically, for any sliding and adhesion edge $\mathscr{S}_{ij}(s)$, $\mathscr{A}_{ij}(s)$ on which (24a) or (24b) are alternatively prescribed, it holds that

$$\left[\!\left[\boldsymbol{u}_{ij\boldsymbol{t}}(\boldsymbol{x},s)\right]\!\right]_{\mathscr{S}_{ij}(s)} = \left[\boldsymbol{u}^{(\mathrm{a})}_{ij\boldsymbol{t}}(\boldsymbol{x},t)-\boldsymbol{u}^{(\mathrm{s})}_{ij\boldsymbol{t}}(\boldsymbol{x},t)\right]\Big|_{\mathscr{S}_{ij}(s)} = \boldsymbol{0}, \tag{24a}$$

$$\left[\!\left[\boldsymbol{u}_{ij\boldsymbol{t}}(\boldsymbol{x},t)\right]\!\right]_{\mathscr{A}_{ij}(s)} = \left[\boldsymbol{u}^{(\mathrm{s})}_{ij-1\boldsymbol{t}}(\boldsymbol{x},t)-\boldsymbol{u}^{(\mathrm{a})}_{ij\boldsymbol{t}}(\boldsymbol{x},t)\right]\Big|_{\mathscr{A}_{ij}(s)} = \boldsymbol{0}. \tag{24b}$$

On the other hand, any adhesion edge $\mathscr{A}_{ij}(s)$ on which the BCs (17) are not prescribed must instead originate from the intersection of a previous adhesion solution with the friction parabola $\mu q_z(\boldsymbol{x},s)$, and hence must be continuous with the previous sliding solution (see, for example, Figs. 3 and 4 in [16]). Thus, all the summations in (23) vanish and it immediately follows that

$$\frac{1}{2}V_{\mathrm{r}}(s)\iint_{\mathscr{P}}\frac{\partial}{\partial s}\left[\boldsymbol{q_t}(\boldsymbol{x},s)\cdot\boldsymbol{u_t}(\boldsymbol{x},s)\right]\mathrm{d}\boldsymbol{x} = \frac{1}{2}V_{\mathrm{r}}(s)\frac{\mathrm{d}}{\mathrm{d}s}\iint_{\mathscr{P}}\boldsymbol{q_t}(\boldsymbol{x},s)\cdot\boldsymbol{u_t}(\boldsymbol{x},s)\,\mathrm{d}\boldsymbol{x} \triangleq \frac{1}{2}\dot{W}^{(\epsilon)}(s). \tag{25}$$

In analogy to Eq. (21), the second integral showing in Eq. (19) gives

$$V_{\mathrm{r}}(s)\iint_{\mathscr{P}}\boldsymbol{q_t}(\boldsymbol{x},s)\cdot\left(\boldsymbol{v_t}(\boldsymbol{x},s)\cdot\nabla_{\boldsymbol{t}}\right)\boldsymbol{u_t}(\boldsymbol{x},s)\,\mathrm{d}\boldsymbol{x} = \frac{1}{2}V_{\mathrm{r}}(s)\iint_{\mathscr{P}}\left(\bar{\boldsymbol{v}}_{\boldsymbol{t}}(\boldsymbol{x},s)\cdot\nabla_{\boldsymbol{t}}\right)\left[\boldsymbol{q_t}(\boldsymbol{x},s)\cdot\boldsymbol{u_t}(\boldsymbol{x},s)\right]\mathrm{d}\boldsymbol{x}. \tag{26}$$

Integrating by parts the integral on the right-hand side of Eq. (26) yields

$$\begin{aligned}\iint_{\mathscr{P}}\bar{\boldsymbol{v}}_{\boldsymbol{t}}(\boldsymbol{x},s)\cdot\nabla_{\boldsymbol{t}}\left[\boldsymbol{q_t}(\boldsymbol{x},s)\cdot\boldsymbol{u_t}(\boldsymbol{x},s)\right]\mathrm{d}\boldsymbol{x} &= -\iint_{\mathscr{P}}\boldsymbol{q_t}(\boldsymbol{x},s)\cdot\boldsymbol{u_t}(\boldsymbol{x},s)\nabla_{\boldsymbol{t}}\cdot\bar{\boldsymbol{v}}_{\boldsymbol{t}}(\boldsymbol{x},s)\,\mathrm{d}\boldsymbol{x}\\ &+\sum_{i\in\mathcal{I}}\sum_{j\in\mathcal{J}_i}\oint_{\partial\mathscr{P}^{(\mathrm{a})}_{ij}(s)}\left[\boldsymbol{q}^{(\mathrm{a})}_{ij\boldsymbol{t}}(\boldsymbol{x},s)\cdot\boldsymbol{u}^{(\mathrm{a})}_{ij\boldsymbol{t}}(\boldsymbol{x},s)\right]\bar{\boldsymbol{v}}_{\boldsymbol{t}}(\boldsymbol{x},s)\cdot\hat{\boldsymbol{\nu}}_{\partial\mathscr{P}^{(\mathrm{a})}_{ij}}(\boldsymbol{x},s)\,\mathrm{d}L\\ &+\sum_{i\in\mathcal{I}}\sum_{j\in\mathcal{J}_i}\oint_{\partial\mathscr{P}^{(\mathrm{s})}_{ij}(s)}\left[\boldsymbol{q}^{(\mathrm{s})}_{ij\boldsymbol{t}}(\boldsymbol{x},s)\cdot\boldsymbol{u}^{(\mathrm{s})}_{ij\boldsymbol{t}}(\boldsymbol{x},s)\right]\bar{\boldsymbol{v}}_{\boldsymbol{t}}(\boldsymbol{x},s)\cdot\hat{\boldsymbol{\nu}}_{\partial\mathscr{P}^{(\mathrm{s})}_{ij}}(\boldsymbol{x},s)\,\mathrm{d}L.\end{aligned} \tag{27}$$

Similarly to what done before, Eq. (27) may be simplified by analysing each integral contribution separately. In particular, the first term on the right-hand side vanishes since the velocity field $\bar{\boldsymbol{v}}_{\boldsymbol{t}}(\boldsymbol{x},s)$ in (3) is solenoidal, that is $\nabla_{\boldsymbol{t}}\cdot\bar{\boldsymbol{v}}_{\boldsymbol{t}}(\boldsymbol{x},s)=0$. The terms in the summations which belong to $\partial\mathscr{P}$ or separate a domain $\mathscr{P}_{ij}$ from the adjacent domains $\mathscr{P}_{i+1j}$ or $\mathscr{P}_{i-1j}$ also disappear for the reasons already discussed. Therefore, Eq. (27) gives

$$\begin{aligned}&\iint_{\mathscr{P}}\bar{\boldsymbol{v}}_{\boldsymbol{t}}(\boldsymbol{x},s)\cdot\nabla_{\boldsymbol{t}}\left[\boldsymbol{q_t}(\boldsymbol{x},s)\cdot\boldsymbol{u_t}(\boldsymbol{x},s)\right]\mathrm{d}\boldsymbol{x} =\\ &+\sum_{i\in\mathcal{I}}\sum_{j\in\mathcal{J}_i}\int_{\mathscr{S}_{ij}(s)}\left[\!\left[\boldsymbol{q}_{ij\boldsymbol{t}}(\boldsymbol{x},s)\cdot\boldsymbol{u}_{ij\boldsymbol{t}}(\boldsymbol{x},s)\right]\!\right]_{\mathscr{S}_{ij}(s)}\bar{\boldsymbol{v}}_{\boldsymbol{t}}(\boldsymbol{x},s)\cdot\hat{\boldsymbol{\nu}}_{\mathscr{S}_{ij}}(\boldsymbol{x},s)\,\mathrm{d}L,\\ &+\sum_{i\in\mathcal{I}}\sum_{j\in\mathcal{J}_i|j>1}\int_{\mathscr{A}_{ij}(s)}\left[\!\left[\boldsymbol{q}_{ij\boldsymbol{t}}(\boldsymbol{x},s)\cdot\boldsymbol{u}_{ij\boldsymbol{t}}(\boldsymbol{x},s)\right]\!\right]_{\mathscr{A}_{ij}(s)}\bar{\boldsymbol{v}}_{\boldsymbol{t}}(\boldsymbol{x},t)\cdot\hat{\boldsymbol{\nu}}_{\mathscr{A}_{ij}}(\boldsymbol{x},s)\,\mathrm{d}L=0,\end{aligned} \tag{28}$$

where the last identities stem again from the BCs (24a) and (24b), respectively. Hence, the final expression for the total power generated during the transient manoeuvre is, in compact notation,

$$P_{\mathrm{s}}(s) = \frac{1}{2}\dot{W}^{(\epsilon)}(s) - P_{\boldsymbol{\sigma}}(s) - P_{\varphi}(s) + P^{(\epsilon)}_{\gamma}(s). \tag{29}$$

In (29), the following separate contributions may be identified

1. $W^{(\epsilon)}(s)$: it may be interpreted as an extra amount of frictional work due to the instantaneous deformation of the bristle. Indeed, this term represents the total variation of energy of the contact patch with respect to the initial (undeformed) configuration. If the stiffness matrix $\mathbf{K}_{\boldsymbol{t}}$ is positive definite (semidefinite), this amount is always positive (nonnegative). The additional term $\dot{W}^{(\epsilon)}(s)$ appearing in Eq. (29) accounts therefore for its variation in time, and is due to the fact that the deformations and stresses have not reached their steady-state value yet. Basically, this means that the total dissipation is also determined by the previous sliding state, entering in the equations through the initial conditions $\boldsymbol{u}_{\boldsymbol{t}0}(\boldsymbol{x})$ transported over the contact patch. When the transient is extinguished, the derivative $\dot{W}^{(\epsilon)}(s)$ vanishes and the power losses only depend on the current slip and spin values, as already known from other steady-state analyses. The term $\dot{W}^{(\epsilon)}(s)$ may be also interpreted as an amount of slip power which is used to reach the final deformed state. This aspect is discussed more extensively in Sect. 4.

2. $P_{\boldsymbol{\sigma}}(s)$: the presence of this term is an expected result. It accounts for the dissipation due to the work performed by the tangential force $\boldsymbol{F}_{\boldsymbol{t}}(s)$. Mathematically, this should be intuitive: the tangential forces represent the dual entities of the translational slip $\boldsymbol{\sigma}(s)$.

3. $P_{\varphi}(s)$: analogous as previously, this terms is due to the power dissipation related to the work performed by the self-aligning moment $M_z(s)$ on the total deformed configuration (including the deflection of the bristle as in (7b)). The self-aligning moment is therefore interpreted as the dual entity of the spin $\varphi(s)$. From a physical perspective, it could be asserted that the (generalised) forces only perform work for the corresponding (generalised) displacements.

4. $P_{\gamma}^{(\epsilon)}(s)$: this quantity appears to be new. It only accounts for the power generated due to the geometric spin (camber) with respect to the bristle deflection. It has opposite sign to the previous term $P_{\varphi}(s)$, meaning that the camber does not cause any frictional losses on the final deformed configuration, but performs work only on the initial one. In fact, it is also possible to write $-P_{\varphi}(s) + P_{\gamma}^{(\epsilon)}(s) = -P_{\psi}(s) - P_{\gamma}^{(0)}(s)$, where $P_{\psi}(s)$ is the total frictional loss due to the turn spin $\dot{\psi}$ computed on the final (deformed) configuration, whilst $P_{\gamma}^{(0)}(s)$ is the power loss due to camber on the initial undeformed configuration. This result may be interpreted by observing that the spin component due to camber does not contribute to the sliding velocity of the tip of the bristle contacting the ground, and hence does not dissipate power with respect to the final deformed state. This is a direct consequence of the fact that the road is modelled as a perfect rigid body, and hence the rotational component of the tip of a bristle contacting the ground does not depend explicitly on the camber angle. The presence of the term $P_{\gamma}^{(\epsilon)}(s)$ in (29) is symptomatic of the fact that, when the camber angles are sufficiently large, the turn and geometric spin must be treated separately, since they are responsible for different phenomena. On the other hand, when the total spin is small enough to justify the resort to the classic theory, it is possible to approximate the computation of $M_z(s)$ integrating on the reference configuration, and thus $P_{\mathrm{s}}(s) \simeq \frac{1}{2}\dot{W}^{(\epsilon)}(s) - P_{\boldsymbol{\sigma}}(s) - P_{\varphi}(s)$, with $P_{\varphi}(s)$ taking into account the contribution of the total spin $\varphi(s) = \varphi_{\psi}(s) + \varphi_{\gamma}(s)$.

It is worth noticing that Eq. (29) may be used to compute the tyre slip losses $P_{\mathrm{s}}(s)$ even when the tangential forces are approximated by integrating the adhesion solution over the contact patch. Of fundamental importance is also to highlight that, according to (29), the equivalence between the macro and micro approaches may only be established in steady-state conditions. Indeed, the term $\frac{1}{2}\dot{W}^{(\epsilon)}(s)$ cannot be deduced directly from global equilibrium considerations.

To conclude, it should be noticed that the new terms $W^{(\epsilon)}(s)$ and $P_{\gamma}^{(\epsilon)}(s)$ do not consider solely the contributions due to the sliding velocities of the tip of the bristles contacting the ground. Indeed, they explicitly account for the deformation of the bristles. Therefore, they might be related to losses phenomena which take place inside the rubber material. In fact, although the bristles are assumed to be infinitesimal in the brush model, they represent the tyre tread.

4 Results and discussion

To exemplify the theory developed in Sect. 3, a simple application is illustrated which deals with an initial undeformed distribution of the bristles inside the contact patch. The contact geometry and the pressure distribution are modelled as in Example 2.3. Introducing a local coordinate system

Table 1: Tyre parameters

Parameter	Description	Unit	Value
C_σ	Slip stiffness	N	$6 \cdot 10^4$
F_z	Vertical force	N	6000
R_r	Rolling radius	m	0.3
a	Contact patch length	m	0.045
b	Contact patch width	m	0.035
Ω	Rolling speed	$\mathrm{rad\,s^{-1}}$	30
μ	Friction coefficient	-	1
σ	Total translational slip	-	0.14
σ^cr	Critical slip	-	0.3

$\boldsymbol{\xi} = (\xi, \eta, \zeta) = (a - x, y, z)$, and the IC may be thus stated mathematically as $\boldsymbol{u}_{\boldsymbol{t}0}(\boldsymbol{\xi}) = \boldsymbol{0}$. An isotropic tyre subjected to small translational slips $\boldsymbol{\sigma}$ is finally considered, for which closed-form solutions are already known from the literature [16, 18]. These conditions are typical for heavy-duty vehicles travelling at relatively low speed and approaching curves with limited slip angles. Since truck tyres are mounted with almost no camber ($\varphi_\gamma \simeq \varphi_\psi \simeq \varphi \simeq 0$), the mathematical treatment may be simplified by considering a one-dimensional, constant velocity field $\bar{\boldsymbol{v}}_{\boldsymbol{t}}(\boldsymbol{\xi}) = -\hat{\boldsymbol{e}}_x$ inside the contact patch. In this way, the rectangular contact shape and the parabolic pressure distribution in Example 2.3 automatically satisfy Assumption 2.2.

With the premises above, under vanishing sliding conditions, the solution to (2) reads

$$\boldsymbol{u}_{\boldsymbol{t}}^{-}(\boldsymbol{\xi}) = \boldsymbol{\sigma}\xi, \qquad (\boldsymbol{\xi}, s) \in [0, s) \times [-b, b] \times \mathbb{R}_{\geq 0}, \tag{30a}$$

$$\boldsymbol{u}_{\boldsymbol{t}}^{+}(\boldsymbol{\xi}, s) = \boldsymbol{\sigma}s, \qquad (\boldsymbol{\xi}, s) \in [s, 2a] \times [-b, b] \times \mathbb{R}_{\geq 0}. \tag{30b}$$

It follows automatically that $\mathscr{P}^-$ and $\mathscr{P}^+$ correspond to the domain of definitions of $\boldsymbol{u}_{\boldsymbol{t}}^{-}(\boldsymbol{\xi})$ and $\boldsymbol{u}_{\boldsymbol{t}}^{+}(\boldsymbol{\xi}, s)$, respectively. Denoting the bristle stiffnesses by $k_{xx} = k_{xy} = k$, the tangential stress vector inside the contact patch reads $\boldsymbol{q}_{\boldsymbol{t}}(\boldsymbol{\xi}, s) = k\boldsymbol{u}_{\boldsymbol{t}}(\boldsymbol{\xi}, s)$ and is therefore oriented as the deformation. Once the shear stress exceeds the friction parabola, the constant[10] sliding solution is given by $\boldsymbol{u}_{\boldsymbol{t}}^{(\mathrm{s})} = \frac{\mu}{k} q_z(\boldsymbol{\xi}) \frac{\boldsymbol{\sigma}}{\sigma}$, where $\sigma = \|\boldsymbol{\sigma}\|$.

Figure 2 shows the trend of the total shear stress $q_{\boldsymbol{t}}(\boldsymbol{\xi}, s) = \big\|\boldsymbol{q}_{\boldsymbol{t}}(\boldsymbol{\xi}, s)\big\|$ for three different values of the nondimensional travelled distance $\bar{s} = s/(2a)$ and versus the nondimensional longitudinal coordinate $\bar{\xi} = \xi/(2a)$. The tyre parameters used for the simulation of Fig. 2 are listed in Tab. 1. The bristle stiffness may be deduced from the slip stiffness C_σ as $k = C_\sigma/(4a^2 b)$. It may be noticed that the total stress increases as the tyre keeps rolling, until the transient vanishes. The time-varying sliding edge $\mathscr{S}(s)$ (or breakaway point) travels backward with increasing longitudinal speed given by

$$\bar{\boldsymbol{v}}_{\mathscr{S}}^{(\hat{\boldsymbol{\nu}})}(s) = -\frac{\sigma}{\sigma^\mathrm{cr}\sqrt{1 - \dfrac{2\sigma s}{a\sigma^\mathrm{cr}}}}\hat{\boldsymbol{e}}_x, \tag{31}$$

and the transient extinguishes as soon as the nondimensional travelled distance $\bar{s}$ equals the breakaway point in steady-state conditions. This is in accordance with theoretical results also presented by Kalker [23–26]. In general, once sliding conditions occur, adhesion is never restored. This happens for any concave pressure distribution, provided that the total slip is less sufficiently smaller than the critical value[11], and in particular $\sigma \leq \sigma^\mathrm{cr}/2$. The central and bottom plots in Fig. 2 illustrate the trend of the total sliding velocity $v_\mathrm{s}(\boldsymbol{\xi}, s) = \big\|\boldsymbol{v}_\mathrm{s}(\boldsymbol{\xi}, s)\big\|$ and the power density loss for unit of area $p_\mathrm{s}(\boldsymbol{\xi}, s)$ due to pure translational slip conditions. It is obvious that, since sliding only takes place in $\mathscr{P}^{(\mathrm{s})}$, the energy is only dissipated in the sliding zone, as also remarked in [15]. However, from the global equilibrium of Eq. (29), it may be inferred that is the total force generated over the whole contact patch to work for the macroscopic slip variable.

Figure 3 shows the different power contributions generated during the transient rolling of the tyre from the initial state to a travelled distance which equals the contact patch length. It may be observed that the two terms $-P_{\boldsymbol{\sigma}}(s)$ and $\frac{1}{2}\dot{W}^{(\epsilon)}(s)$ have opposite sign. For an isotropic tyre subjected to pure

[10] The sliding solution is independent of the time provided that the vertical pressure distribution is also at steady-state.

[11] For a rectangular contact patch, the critical slip value is defined as $\mu|\partial q_z(0)/\partial\xi|$. The notion may be generalised to other shapes, as discussed extensively in [18].

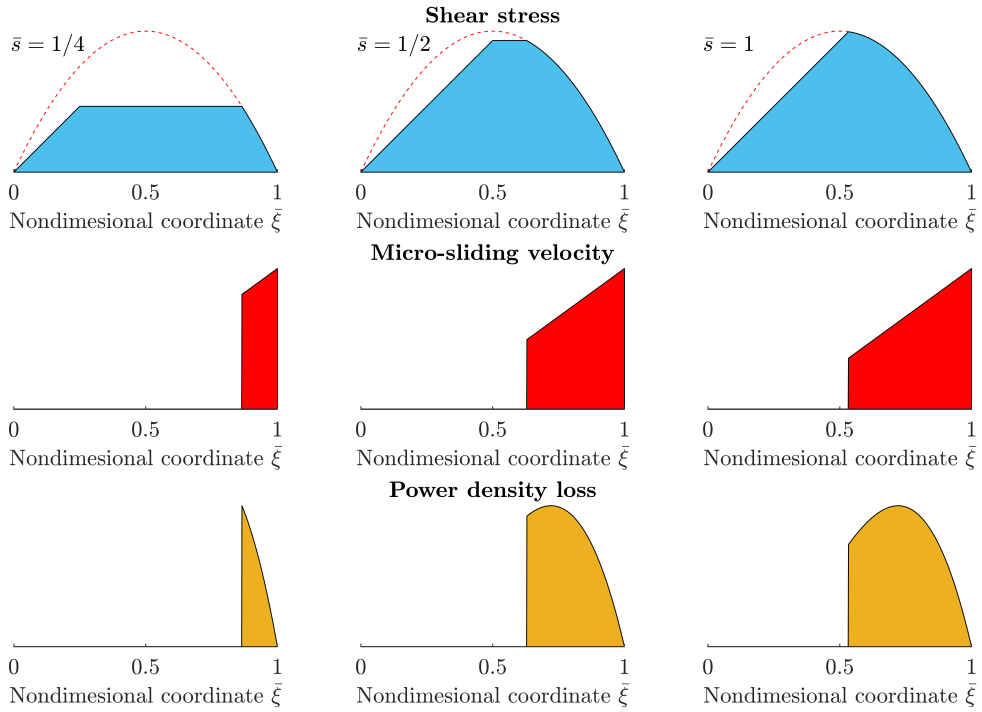

Figure 2: Transient distribution of the shear stresses, micro-sliding velocity and power density losses inside the contact patch for three different values of the nondimensional travelled distance $\bar{s} = 1/4$, $1/2$ and 1, respectively. The power is only dissipated in the sliding zone, and the transient extinguishes as soon as the travelled distance equals the position of the steady-state breakaway point.

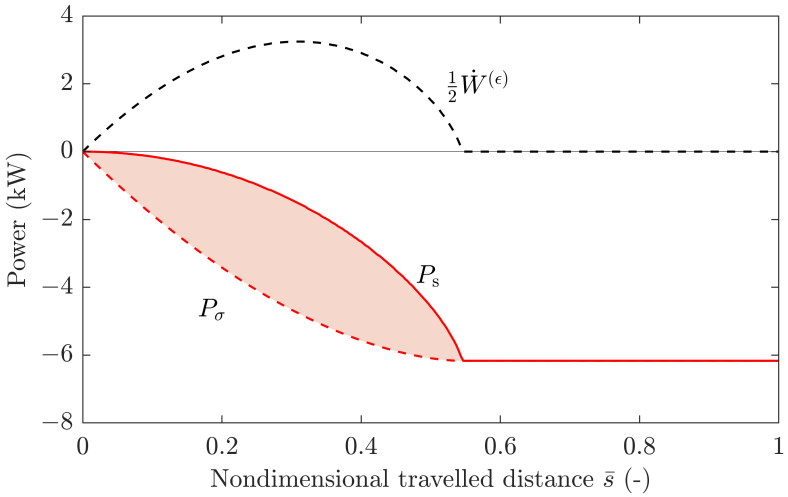

Figure 3: Trend of the power slip losses against the nondimensional travelled distance $\bar{s} = s/(2a)$. The two terms $P_{\boldsymbol{\sigma}}$ and $\frac{1}{2}\dot{W}$ contribute differently to the total dissipation P_{s}. In particular, $-P_{\boldsymbol{\sigma}}$ produces an effective energy loss as the tyre keeps rolling, whilst $\frac{1}{2}\dot{W}$ introduces extra energy which is used to reach the current deformed configuration.

translational slip, $-P_{\boldsymbol{\sigma}}(s)$ (dashed red line) is always negative, since the shear stresses $\boldsymbol{q}_{\boldsymbol{t}}(\boldsymbol{\xi}, s)$ have the same direction of the bristle deflection[12]. This results in an expected dissipation, since the total force exerted at the tyre-road interface opposes the rolling of the wheel. On the other hand, the amount $\dot{W}^{(\epsilon)}(s)$ may be concordant or discordant with $P_{\boldsymbol{\sigma}}(s)$. For the case under consideration, the derivative $\dot{W}^{(\epsilon)}(s)$ (dashed black line) is positive, since the bristles are accumulating deformation energy as the travelled distance s increases. This energy is stored in the contact patch and converted into a propelling force $\boldsymbol{F}_{\boldsymbol{t}}(s)$. In fact, the bristles are undergoing a transient from the undeformed initial state $\boldsymbol{u}_{\boldsymbol{t}0}(\boldsymbol{\xi})$ to a new deformed configuration. If the bristles in their initial configuration had been subjected to larger deflections with respect to the steady-state value, then $\dot{W}(s)$ would have contributed to dissipating power together with the term $-P_{\boldsymbol{\sigma}}(s)$. Obviously, $-P_{\boldsymbol{\sigma}}(s)$ and $P_{\mathrm{s}}(s)$ (solid red line) converge to the same value once the transient is extinguished, since the derivative $\dot{W}(s)$ vanishes as soon as the travelled distance equals the position of the steady-state breakaway point. The light red area shown in Fig. 3 represents qualitatively the difference between the dissipated energy calculated with and without taking into account the additional contribution due to $\frac{1}{2}\dot{W}^{(\epsilon)}(s)$. In numbers, this amounts to $1.22 \cdot 10^{-2}$ kJ, corresponding to nearly 33% of the total dissipation. Clearly, this represents a conspicuous amount of the total slip losses, and must be properly considered.

From the above example it emerges that, in transient conditions, the conventional approximation $P_{\mathrm{s}}(s) = -P_{\boldsymbol{\sigma}}(s)$ might misestimate the real losses. Indeed, the effect of the transient deformation of the tyre tread would become particularly significant at every change in local slip conditions caused by cornering, acceleration, braking manoeuvres and modifications of the camber angle as a consequence of the reaction of the vehicle suspension. It is, however, extremely difficult to account for the term $\frac{1}{2}\dot{W}^{(\epsilon)}(s)$, especially when describing the tyre forces by means of empirical models, such as Pacejka's Magic Formula. This is the standard approach in vehicle dynamics simulations, where the brush models are usually replaced with more sophisticated formulations which are able to handle critical occurrences as, for example, zero longitudinal slip [4, 27].

5 Conclusions

In the present paper, the authors have analysed the power dissipation connected with tyre slip losses by means of the well-established brush theory. The problem has been formulated in very general terms, considering unsteady phenomena and a two-dimensional velocity field inside the contact patch due to the presence of large camber angles. The investigation has been mainly based on some recent studies conducted by the authors [16–18]. In particular, the analytical expression for the slip losses taking

[12] At least if the initial conditions are also oriented as the slip $\boldsymbol{\sigma}$.

place at the tyre-road interface has been derived starting from the transient transport equations for the micro-sliding velocity. This allowed to cope with the problem without solving the aforementioned PDEs for a specific contact shape or pressure distribution, as done instead in previous studies [15]. Furthermore, the results established in this paper are only grounded on few reasonable assumptions, which reflect the physical nature of the phenomenon. Therefore, the claims advocated in this paper may be regarded as general.

In particular, two important findings which appear to be new have been highlighted in this paper. The first one relates to the contribution of the self-aligning moment to the overall slip losses. Indeed, it emerges from the present analysis that, when the camber angles are sufficiently large, the geometric spin does not perform work on the deformed configuration of the tyre. This is due to the fact that the velocity field of the tip of a bristle contacting the ground is unaffected by the rotational component of the speed due to camber. On the other hand, the turn spin produces a dissipation which must be computed on the deformed configuration, i.e. considering the additional lever resulting from the displacement of the bristle where the shear stress is applied.

The second result connects to the additional contribution to the slip losses due to the transient phenomena taking place during the rolling of the tyre. It is shown in the present investigation that the time variation of the total energy stored in the contact patch also produces a significant effect on the total dissipation. A numerical example has been proposed to quantify this energy release subsequent to a translational slip input. It has been found that the discrepancy in prediction by only considering the negative work performed by the tangential forces for the corresponding slip amounts to nearly 42% of the total dissipation. In conclusion, it appears that the conventional ways of calculating the slip losses are inadequate when dealing with severe transients, and might eventually lead to large misestimations. This might be a problem, especially in the context of vehicle dynamics simulations, where energy efficiency is often assessed by approximating the tyre forces with their steady-state value. Future work shall thus be devoted to developing simplified models for tyre slip losses able to capture these complex phenomena. A possible way of taking into account the additional contribution from the transient phases could be to incorporate the non-steady terms in a rolling resistance model, since these appear to describe dissipation phenomena which may happen inside the rubber material. Another direction which is worth exploring relates to the possibility of including damping effects in the constitutive relationship for the tyre tread. This would certainly impact the term $\dot{W}^{(\epsilon)}(s)$ introduced in this paper.

Acknowledgements

The authors gratefully acknowledge financial support from the COVER project (44929-1), funded by the Swedish energy agency and the Swedish vehicle research and innovation program (FFI).

Compliance with Ethical Standards

The authors declare that they have no conflict of interest.

Nomenclature

Forces and Moments	**Unit**	**Description**
$\boldsymbol{q_t}$	$\mathrm{N\,m^{-2}}$	Tangential shear stress vector
q_t	$\mathrm{N\,m^{-2}}$	Total tangential shear stress
q_x, q_y	$\mathrm{N\,m^{-2}}$	Longitudinal and lateral shear stress
$\boldsymbol{q_t}^{(\mathrm{a})}$	$\mathrm{N\,m^{-2}}$	Tangential shear stress vector in the adhesion zone
$q_x^{(\mathrm{a})}$, $q_y^{(\mathrm{a})}$	$\mathrm{N\,m^{-2}}$	Longitudinal and lateral shear stress in the adhesion zone
$\boldsymbol{q_t}^{(\mathrm{s})}$	$\mathrm{N\,m^{-2}}$	Tangential shear stress vector in the sliding zone
$q_x^{(\mathrm{s})}$, $q_y^{(\mathrm{s})}$	$\mathrm{N\,m^{-2}}$	Longitudinal and lateral shear stresses in the sliding zone
q_z	$\mathrm{N\,m^{-2}}$	Vertical pressure
q_z^*	$\mathrm{N\,m^{-2}}$	Reference value for the vertical pressure
$\boldsymbol{F_t}$	N	Tangential force vector

F_x, F_y, F_z	N	Longitudinal, lateral and vertical tyre forces
M_z	N m	Self-aligning moment

Displacements	**Unit**	**Description**
$\boldsymbol{u_t}$	m	Displacement vector of the bristle
u_x, u_y	m	Longitudinal and lateral displacement of the bristle
$\boldsymbol{u_t}^{(\mathrm{a})}$	m	Displacement vector of the bristle in the adhesion zone
$u_x^{(\mathrm{a})}$, $u_y^{(\mathrm{a})}$	m	Longitudinal ad lateral displacement in the adhesion zone
$\boldsymbol{u_t}^{(\mathrm{s})}$	m	Displacement vector of the bristle in the sliding zone
$u_x^{(\mathrm{s})}$, $u_y^{(\mathrm{s})}$	m	Longitudinal and lateral displacement in the sliding zone
$\boldsymbol{u_{t0}}$	m	Initial tangential displacement vector of the bristle (IC)
u_{x0}, u_{y0}	m	Initial longitudinal and lateral displacement (IC)
s	m	Travelled distance
$\boldsymbol{x}$	m	Coordinate vector
x, y, z	m	Longitudinal, lateral and vertical coordinates
x_0, y_0	m	Initial longitudinal and lateral data (ID)
$\boldsymbol{\xi}$	m	Local coordinate vector
ξ, η, ζ	m	Local longitudinal, lateral and vertical coordinates
$\xi_{\mathscr{S}}$	m	Explicit representation of the sliding edge

Speeds	**Unit**	**Description**
$\bar{\boldsymbol{v}}_{\boldsymbol{t}}$	$\mathrm{m\,s^{-1}}$	Nondimensional tangential velocity field
$\bar{v}_x$, $\bar{v}_y$	$\mathrm{m\,s^{-1}}$	Nondimensional longitudinal and lateral components of the velocity field
$\boldsymbol{v}_{\mathrm{s}}$	$\mathrm{m\,s^{-1}}$	Tangential micro-sliding velocity
$v_{\mathrm{s}x}$, $v_{\mathrm{s}y}$	$\mathrm{m\,s^{-1}}$	Longitudinal and lateral micro-sliding speeds
$\bar{\boldsymbol{v}}_{\mathrm{s}}$	$\mathrm{m\,s^{-1}}$	Nondimensional tangential micro-sliding velocity
$\bar{v}_{\mathrm{s}x}$, $\bar{v}_{\mathrm{s}y}$	$\mathrm{m\,s^{-1}}$	Nondimensional longitudinal and lateral micro-sliding speeds
V_{r}	$\mathrm{m\,s^{-1}}$	Tyre rolling speed
$\dot{\psi}$	$\mathrm{rad\,s^{-1}}$	Steering speed
Ω	$\mathrm{rad\,s^{-1}}$	Angular speed of the rim

Slip Parameters	**Unit**	**Description**
χ_γ, χ_ψ	-	Camber and turning ratio
ε_γ	-	Camber reduction factor
$\boldsymbol{\sigma}$	-	Translational slip vector
σ	-	Total translational slip
σ_x, σ_y	-	Longitudinal and lateral slip
σ^{cr}	-	Critical slip
φ	$\mathrm{m^{-1}}$	Rotational slip or spin parameter
φ_γ, φ_ψ	$\mathrm{m^{-1}}$	Camber and turning spin parameters

Rotation Matrices and Tensors	**Unit**	**Description**
$\mathbf{A}_\varphi$	$\mathrm{m^{-1}}$	Spin tensor

Geometric Parameters	**Unit**	**Description**
γ	rad	Camber angle

Stiffnesses and Compliances	**Unit**	**Description**
$\mathbf{K}_{\boldsymbol{t}}$	$\mathrm{N\,m^{-3}}$	Matrix of the bristle tangential stiffnesses

$k_{xx} = k_{yy} = k$	$\mathrm{N\,m^{-3}}$	Bristle longitudinal and lateral stiffnesses
C_σ	N	Slip stiffness

Friction Parameters	**Unit**	**Description**
μ	-	Friction coefficient

Powers and Energies	**Unit**	**Description**
p_s	$\mathrm{W\,m^{-2}}$	Slip losses per unit of area
P_s	W	Total slip losses
$P_{\boldsymbol{\sigma}}$	W	Power dissipated by the translational slip
P_φ	W	Power dissipated by the spin slip
$P_\gamma^{(\epsilon)}$	W	Power compensation on the deformed configuration due to camber
$\dot{W}^{(\epsilon)}$	W	Frictional work due to transient effects

Functions and Operators	**Unit**	**Description**
$\nabla_{\boldsymbol{t}}$	$\mathrm{m^{-1}}$	Tangential gradient

Sets	**Unit**	**Description**
$\mathit{\Pi}$	$\mathrm{m^2}$	Road plane
$\mathscr{P}$	$\mathrm{m^2}$	Contact patch
$\mathscr{P}^{(\mathrm{a})}$	$\mathrm{m^2}$	Adhesion zone
$\mathscr{P}^{(\mathrm{s})}$	$\mathrm{m^2}$	Sliding zone
$\mathring{\mathscr{P}}$	$\mathrm{m^2}$	Interior of $\mathscr{P}$
$\partial\mathscr{P}$	m	Boundary of $\mathscr{P}$
$\mathscr{A}$	m	Adhesion edge
$\mathscr{L}$	m	Leading edge
$\mathscr{N}$	m	Neutral edge
$\mathscr{S}$	m	Sliding edge
$\mathscr{T}$	m	Trailing edge
$\mathbb{R}_{\geq 0}$	-	Set of positive real numbers (including 0)
$\mathbb{R}_{>0}$	-	Set of strictly positive real numbers (excluding 0)

References

[1] Beckers CJJ, Besselink IJM, Nijmeijer H. Modeling of Energy Losses During Cornering for Electric City Buses. 2019 IEEE Intelligent Transportation Systems Conference (ITSC), Auckland, New Zealand. 2019;164-4169. Available from: https://doi.org/10.1109/ITSC.2019.8917232.

[2] Beckers C, Besselink IJM, Nijmeijer H. Assessing the impact of cornering losses on the energy consumption of electric city buses. Transportation Research Part D: Transport and Environment. 2020;86. Available from: https://doi.org/10.1016/j.trd.2020.102360.

[3] Suzuki Y, Kano Y, Abe M. A study on tyre force distribution controls for full drive-by-wire electric vehicle. Veh Syst Dyn. 2014;52:235–250.

[4] Pacejka HB. Tire and vehicle dynamics. 3rd ed. Amsterdam: Elsevier/BH; 2012.

[5] Guiggiani M. The Science of Vehicle Dynamics, 2nd ed. Cham(Switzerland): Springer International; 2018.

[6] Limebeer DJN, Massaro M. Dynamics and Optimal Control of Road Vehicle. Oxford University Press; 2018.

[7] Romano L. Advanced Brush Tyre Modelling. 1st ed. Springer Cham; 2022. Available from: https://doi.org/10.1007/978-3-030-98435-9.

[8] Gruber P, Sorniotti A, Lenzo B, et al. Energy efficient torque vectoring control. Advanced Vehicle Control (Proceedings of AVEC'16) CRC Press; 2016.

[9] Kobayashi T, Katsuyama E, Sugiura H, et al. Direct yaw moment control and power consumption of in-wheel motor vehicle in steady state turning. Veh Syst Dyn. 2017;55(1):104–120. Available from: https://doi.org/10.1080/00423114.2016.1246737.

[10] Kobayashi T, Katsuyama E, Sugiura H, et al. Efficient direct yaw moment control: tyre slip power loss

minimization for four-independent wheel drive vehicle. Veh Syst Dyn. 2018;56(5):719–733. Available from: https://doi.org/10.1080/00423114.2017.1330483.
[11] Torinsson J, Jonasson M, Yang D, Jacobson B. Energy reduction by power loss minimisation through wheel torque allocation in electric vehicles: a simulation-based approach. Vehicle Syst. Dyn. Available from: https://doi.org/10.1080/00423114.2020.1858121.
[12] Alarcón GI, Burgelman N, Meza JM, Toro A, Li Z. The influence of rail lubrication on energy dissipation in the wheel/rail contact: A comparison of simulation results with field measurements. Wear. 2015;330–331:533-539. Available from: https://doi.org/10.1016/j.wear.2015.01.008.
[13] Alarcón GI, Burgelman N, Meza JM, Toro A, Li Z. Power dissipation modeling in wheel/rail contact: Effect of friction coefficient and profile quality. Wear. 2016;366–367:217-224. Available from: https://doi.org/10.1016/j.wear.2016.04.026.
[14] Burgelman N. The Wheel-Rail Contact Problem in Vehicle System Dynamic Simulation (PhD thesis) Delft University of Technology, The Netherlands (2016).
[15] Kobayashi T, Katsuyama E, Sugiura H, Hattori H, Ono E, Yamamoto M. Theoretical analysis of tyre slip power dissipation mechanism using brush model. Vehicle Syst. Dyn. 2020;58(8):1242-1256. Avaliable from https://doi.org/10.1080/00423114.2019.1612926.
[16] Romano L, Bruzelius F Jacobson B. Unsteady-state brush theory. Vehicle Syst. Dyn. 2020; pages 1-29. Available from: https://doi.org/10.1080/00423114.2020.1774625.
[17] Romano L, Bruzelius F, Jacobson B. Brush tyre models for large camber angles and steering speeds. Vehicle System Dynamics. Available from: https://doi.org/10.1080/00423114.2020.1854320.
[18] Romano L, Timpone F, Bruzelius F, Jacobson B. Analytical results in transient brush tyre models: theory for large camber angles and classic solutions with limited friction. Meccanica 57, 165–191 (2022). Available from: https://doi.org/10.1007/s11012-021-01422-3.
[19] Romano L, Timpone F, Bruzelius F, Jacobson B. Rolling, tilting and spinning spherical wheels: Analytical results using the brush theory. Mechanism and Machine Theory. Volume 173, 2022. Available from: https://doi.org/10.1016/j.mechmachtheory.2022.104836.
[20] Pacejka HB. Spin: camber and turning. Vehicle Syst Dyn. 2005;43(1):3-17. Available from https://doi.org/10.1080/00423110500140013.
[21] Evans LC. Partial differential equations. 2nd ed. American Mathematical Society; 2010.
[22] Ockendon JR, Howison S, Lacey A, Movchan A. Applied partial differential equations. Oxford University Press; 2003.
[23] Kalker JJ. Rolling Contact Phenomena. In: Jacobson B., Kalker J.J. (eds) Rolling Contact Phenomena. International Centre for Mechanical Sciences (Courses and Lectures), vol 411. Springer, Vienna
[24] Kalker JJ. Three-Dimensional Elastic Bodies in Rolling Contact. Springer: Dordrecht; 1990. https://doi.org/10.1007/978-94-015-7889-9.
[25] Kalker JJ. Survey of wheel-rail rolling contact theory. Vehicle Syst Dyn. 1997;8(4):317-358. Available from: https://doi.org/10.1080/00423117908968610 .
[26] Kalker JJ. Transient rolling contact phenomena. ASLE Trans. 1971;14(3):177-184. Available from: https://doi.org/10.1080/05698197108983240.
[27] Pacejka HB, Bakker E. The magic formula tire model. Int. J. Vehicle Mechanics and Mobility, 21(1), 1992, pp. 1-18.
[28] Truesdell C, Toupin RA. The classical field theories. In Flügge S, editor, Handbuch der Physik, vol. 3/1, page 226. Springer-Verag: Berlin; 1960.

A Derivation of a sliding edge velocity

To derive an expression for the velocity of a sliding edge, some basic notions from differential geometry are required. To start, it should be noted that, for a generic $\mathscr{S}_{ij}$, the product $\bar{\boldsymbol{v}}_{\mathscr{S}_{ij}}(\boldsymbol{x},s)\cdot\hat{\boldsymbol{\nu}}_{\mathscr{S}_{ij}}(\boldsymbol{x},s)$ represents the normal component of the velocity of the sliding edge. This may be represented in implicit form as [7]

$$\gamma_{\mathscr{S}_{ij}}(\boldsymbol{x},s)\triangleq\left\|\mathbf{K}_{\boldsymbol{t}}\boldsymbol{u}^{(\mathrm{a})}_{ij\boldsymbol{t}}(\boldsymbol{x},s)\right\|-\mu q_z(\boldsymbol{x},s)=0. \tag{32}$$

The out-ward pointing unit normal to each $\mathscr{S}_{ij}$ is thus given by

$$\hat{\boldsymbol{\nu}}_{\mathscr{S}_{ij}}(\boldsymbol{x},s)=\pm\frac{\nabla_{\boldsymbol{t}}\gamma_{\mathscr{S}_{ij}}(\boldsymbol{x},s)}{\left\|\nabla_{\boldsymbol{t}}\gamma_{\mathscr{S}_{ij}}(\boldsymbol{x},s)\right\|}. \tag{33}$$

Furthermore, differentiating (32) with respect to the travelled distance following a point on the sliding edge yields [28]

$$\frac{\partial \gamma_{\mathscr{S}_{ij}}(\boldsymbol{x},s)}{\partial s} + \bar{\boldsymbol{v}}^{(\boldsymbol{\rho})}_{\mathscr{S}_{ij}}(\boldsymbol{\rho},s)\cdot\nabla_{\boldsymbol{t}}\gamma_{\mathscr{S}_{ij}}(\boldsymbol{x},s) = 0, \tag{34}$$

where the velocity $\bar{\boldsymbol{v}}^{(\boldsymbol{\rho})}_{\mathscr{S}_{ij}}(\boldsymbol{\rho},s)$ is calculated as $\partial f_{\mathscr{S}_{ij}}(\boldsymbol{\rho},s)/\partial s$, where $\boldsymbol{x}(\boldsymbol{\rho},s) = f_{\mathscr{S}_{ij}}(\boldsymbol{\rho},s)$ is a parametric representation of the sliding edge $\gamma_{\mathscr{S}_{ij}}(\boldsymbol{x},s)$. Therefore:

$$\bar{\boldsymbol{v}}^{(\boldsymbol{\rho})}_{\mathscr{S}_{ij}}(\boldsymbol{\rho},s)\cdot\hat{\boldsymbol{\nu}}_{\mathscr{S}_{ij}}(\boldsymbol{x},s) = \bar{\boldsymbol{v}}_{\mathscr{S}_{ij}}(\boldsymbol{x},s)\cdot\hat{\boldsymbol{\nu}}_{\mathscr{S}_{ij}}(\boldsymbol{x},s) = \mp\frac{1}{\left\|\nabla_{\boldsymbol{t}}\gamma_{\mathscr{S}_{ij}}(\boldsymbol{x},s)\right\|}\,\frac{\partial\gamma_{\mathscr{S}_{ij}}(\boldsymbol{x},s)}{\partial s}\,. \tag{35}$$

In particular, the partial derivative $\partial\gamma_{\mathscr{S}_i}(\boldsymbol{x},s)/\partial s$ reads

$$\begin{aligned}\frac{\partial\gamma_{\mathscr{S}_{ij}}(\boldsymbol{x},s)}{\partial s} = {}& \frac{k_{xx}u^{(\mathrm{a})}_{ijx}(\boldsymbol{x},s)+k_{xy}u^{(\mathrm{a})}_{ijy}(\boldsymbol{x},s)}{\left\|\mathbf{K}_{\boldsymbol{t}}\boldsymbol{u}^{(\mathrm{a})}_{ij\boldsymbol{t}}(\boldsymbol{x},s)\right\|}\left(k_{xx}\,\frac{\partial u^{(\mathrm{a})}_{ijx}(\boldsymbol{x},s)}{\partial s}+k_{xy}\,\frac{\partial u^{(\mathrm{a})}_{ijy}(\boldsymbol{x},s)}{\partial s}\right)\\ &+\frac{k_{yx}u^{(\mathrm{a})}_{ijx}(\boldsymbol{x},s)+k_{yy}u^{(\mathrm{a})}_{ijy}(\boldsymbol{x},s)}{\left\|\mathbf{K}_{\boldsymbol{t}}\boldsymbol{u}^{(\mathrm{a})}_{ij\boldsymbol{t}}(\boldsymbol{x},s)\right\|}\left(k_{yx}\,\frac{\partial u^{(\mathrm{a})}_{ijx}(\boldsymbol{x},s)}{\partial s}+k_{yy}\,\frac{\partial u^{(\mathrm{a})}_{ijy}(\boldsymbol{x},s)}{\partial s}\right)-\mu\,\frac{\partial q_z(\boldsymbol{x},s)}{\partial s}\,.\end{aligned} \tag{36}$$

A particular representation of the velocity of a sliding edge which is oriented as the unit normal is thus given by

$$\bar{\boldsymbol{v}}^{(\hat{\boldsymbol{\nu}})}_{\mathscr{S}_{ij}}(\boldsymbol{x},s) \triangleq -\frac{\nabla_{\boldsymbol{t}}\gamma_{\mathscr{S}_{ij}}(\boldsymbol{x},s)}{\left\|\nabla_{\boldsymbol{t}}\gamma_{\mathscr{S}_{ij}}(\boldsymbol{x},s)\right\|^2}\,\frac{\partial\gamma_{\mathscr{S}_{ij}}(\boldsymbol{x},s)}{\partial s}\,. \tag{37}$$

In the following example the above results will be clarified by deriving an explicit representation of the velocity of the sliding edge.

Remark A.1. The above characterisation for the velocity of a sliding edge may be easily extended to a restricted class of adhesion edges. Indeed, any adhesion edge $\mathscr{A}_{ij}$ which originates from the intersection of a previous adhesion solution with the friction parabola $\mu q_z(\boldsymbol{x},s)$ must admit the same implicit representation $\gamma_{\mathscr{A}_{ij}}(\boldsymbol{x},s)$ as in (32), for some (possibly different) index j.

Example A.2 (Rectangular contact patch with combined slip)**.** This example considers again a rectangular contact patch and pure translational slip, with parabolic pressure distribution given by (12). It is assumed to start from zero initial conditions, i.e. $\boldsymbol{u}_{\boldsymbol{t}0}(\boldsymbol{\xi}) = \mathbf{0}$, and thus the bristle displacement in the sliding zone is independent on the travelled distance. Furthermore, small translational slips are considered, i.e. $\sigma = \|\boldsymbol{\sigma}\| < \sigma^{\mathrm{cr}}/2$. This implies the existence of a unique sliding zone, as demonstrated in [16, 18]. Accordingly, an explicit representation of the sliding edge $\xi_{\mathscr{S}}(s)$ may be found as [16]

$$\xi_{\mathscr{S}}(s) = a\left(1+\sqrt{1-\frac{2\sigma s}{a\sigma^{\mathrm{cr}}}}\right), \qquad 0 \le s \le 2a\left(1-\frac{\sigma}{\sigma^{\mathrm{cr}}}\right). \tag{38a}$$

In implicit form, this may be written as

$$\gamma_{\mathscr{S}}(\boldsymbol{\xi},s) = \sigma s - \frac{3\mu F_z}{2aC_\sigma}\xi(2a-\xi) = 0, \tag{39}$$

and thus:

$$\frac{\partial\gamma_{\mathscr{S}}(\boldsymbol{\xi},s)}{\partial s} = \sigma, \tag{40a}$$

$$\frac{\partial\gamma_{\mathscr{S}}(\boldsymbol{\xi},s)}{\partial\xi} = -\frac{3\mu F_z}{aC_\sigma}(a-\xi) = -\frac{\sigma^{\mathrm{cr}}}{a}(a-\xi), \tag{40b}$$

$$\frac{\partial\gamma_{\mathscr{S}}(\boldsymbol{\xi},s)}{\partial\eta} = 0. \tag{40c}$$

Combining Eqs. (40a) and (40b) yields, after some manipulations,

$$\bar{\boldsymbol{v}}^{(\hat{\boldsymbol{\nu}})}_{\mathscr{S}}(s) = -\frac{\nabla_{\boldsymbol{t}}\gamma_{\mathscr{S}}(\boldsymbol{\xi},s)}{\left\|\nabla_{\boldsymbol{t}}\gamma_{\mathscr{S}}(\boldsymbol{\xi},s)\right\|^2}\,\frac{\partial\gamma_{\mathscr{S}}(\boldsymbol{\xi},s)}{\partial s} = -\frac{\sigma}{\sigma^{\mathrm{cr}}\sqrt{1-\dfrac{2\sigma s}{a\sigma^{\mathrm{cr}}}}}\hat{\boldsymbol{e}}_x \equiv \frac{\partial\xi_{\mathscr{S}}(s)}{\partial s}\,\hat{\boldsymbol{e}}_x, \tag{41}$$

where the last identity stems from the fact that the vertical pressure distribution is independent of the lateral coordinate η.